Properties of Near-Surface Inertial Oscillations

R. T. POLLARD

Institute of Oceanographic Sciences, Wormley, Godalming, Surrey, England

(Manuscript received 11 July 1979, in final form 19 October 1979)

ABSTRACT

Inertial oscillations in current records in the top 100 m of the ocean collected on three moorings 50 and 70 km apart are examined. At 12 and 32 m depth the records are horizontally coherent at inertial frequencies and wavelengths between 700 and 1700 km are suggested. At 52 and 72 m depth, records are not horizontally coherent. Vertical wavelengths in the seasonal thermocline lie between 100 and 200 m. Significant differences between the 12 m currents are related to differences in wind over the 50 km spacing, and can be modeled by forcing the Pollard and Millard (1970) model with the local wind. Analysis of the inertial oscillations generated by a well-developed traveling depression suggests that their amplitudes can fall to zero within a few tens of kilometers of the storm track. The waves propagate along paths parallel to the storm track, but form a system of standing waves perpendicular to it. During periods of strong inertial wave generation up to two-thirds of the horizontal kinetic energy in the mixed layer is at near-inertial frequencies. The vertical component of the group velocity in the top 100 m is downward, confirming that the flow of energy is down from the surface.

1. Introduction

It is well established that inertial oscillations in the surface layer of the ocean can be locally generated by changes in the wind (e.g., Gonella, 1971; Schott, 1971; Halpern, 1974), and a simple model (Pollard and Millard, 1970; Pollard *et al.*, 1973; Kundu, 1976; Käse and Olbers, 1979) can describe changes in the amplitude and phase of the forced oscillations quite reasonably.

It is less clear how the energy at near-inertial frequencies is removed from the surface layers. It can disperse through the seasonal thermocline (Pollard, 1970; Kroll, 1975; Käse, 1979) be destroyed again by the wind (Pollard, 1970; Pollard and Millard, 1970) or be converted into higher frequency oscillations that radiate away (Bell, 1978). There is an apparent contradiction between the large (~1000 km) scale of the forcing wind and the small horizontal coherence scales (~50 km) that have been reported (Webster, 1968; Schott, 1971).

To clarify the dispersion process and coherence scales, and to examine the sensitivity of the Pollard and Millard model to small differences in the driving wind field, an experiment was carried out in 1970 while the author was at the Woods Hole Oceanographic Institution. This paper describes the results of that experiment.

2. Experiment and data analysis

For seven weeks in summer 1970 three surface moorings (338, 339 and 340) were set in the vicinity of site D (39°10'N, 70°W) (Fig. 1). Each mooring carried instrumentation to measure horizontal current velocity at depths of 12, 32, 52 and 72 m, and also wind velocity. There was a fifth current meter about 150 m above the bottom (~2600 m) on each mooring, though these will not be discussed further. Of the 18 instruments (Fig. 2) only one (at 32 m on 338) failed entirely, and one (12 m on 338) gave a short record and required extensive editing. A full description of the moorings and data return is given by Pollard and Tarbell (1975).

All the records were at times dominated by inertial oscillations (e.g., Fig. 3, start and end of record) and semidiurnal oscillations were also present (e.g., Fig. 3, around 25 July). Energy spectra (Fig. 4) confirm the dominance of these two frequencies. Fairly distinct minima between four frequency bands—low, inertial, tidal and internal gravity wave—allow one to compare the energy in these four bands (Fig. 5) without serious errors due to the arbitrary choice of partition points.

On all the moorings the total energy is approximately the same at the 52 and 72 m levels, but increases by between two and five times up to the 12 m level. Although the inertial frequency band contributes most to the near-surface increase, the other frequency bands also contribute to it in some cases, which is consistent with Ekman theory [Gonella (1972) where some of these data receive an analysis complementary to that presented here]. In general, 60–80% of the energy is in the low-frequency band (which includes the mean current). Only at the 12 m

0022-3670/80/030385-14$07.50

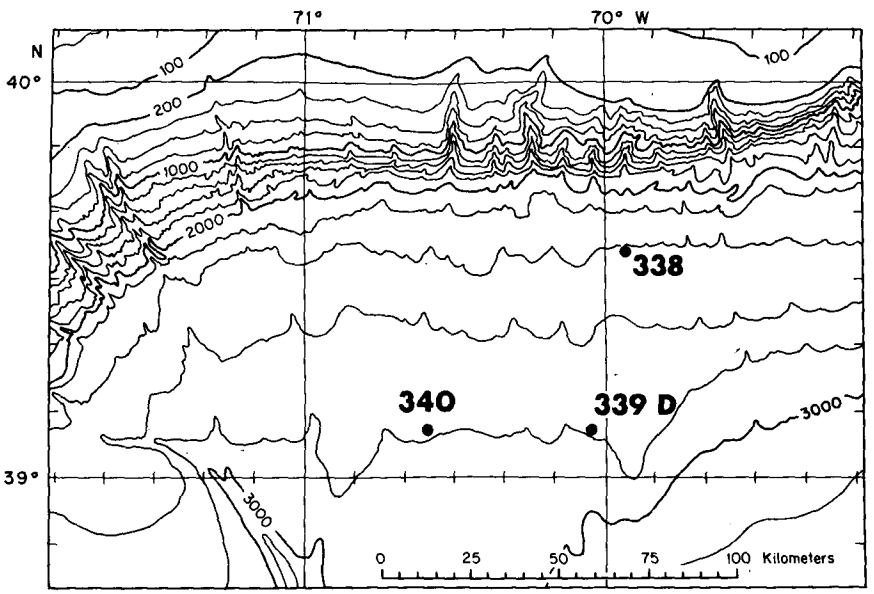

FIG. 1. Approximate bottom topography in the vicinity of site D, showing the positions of the three surface moorings, 338, 339 and 340. Depth contours are marked every 200 m and are labeled in meters. Mooring 338 is about 20 km south of the continental shelf, and the moorings are ~50 km apart in the north–south and east–west directions.

level is the low-frequency energy matched (on two moorings) by the energy in the inertial frequency band.

The computations for Fig. 5 mostly refer to the first 1024 h of data (42.7 days) which includes the period of strong inertial oscillations at the start of the records and also the period of weaker oscillations that followed. To isolate a period in which

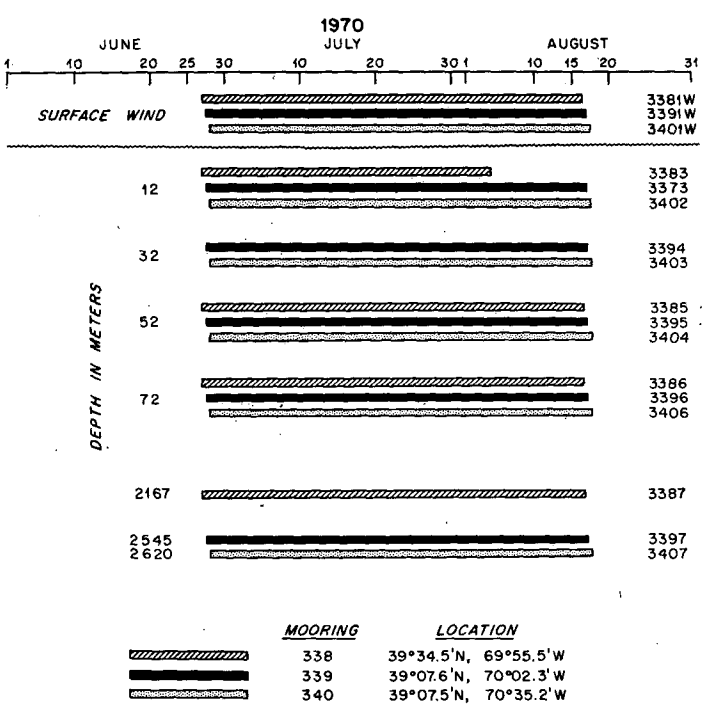

FIG. 2. Locations, instrument depths and record durations on the three moorings.

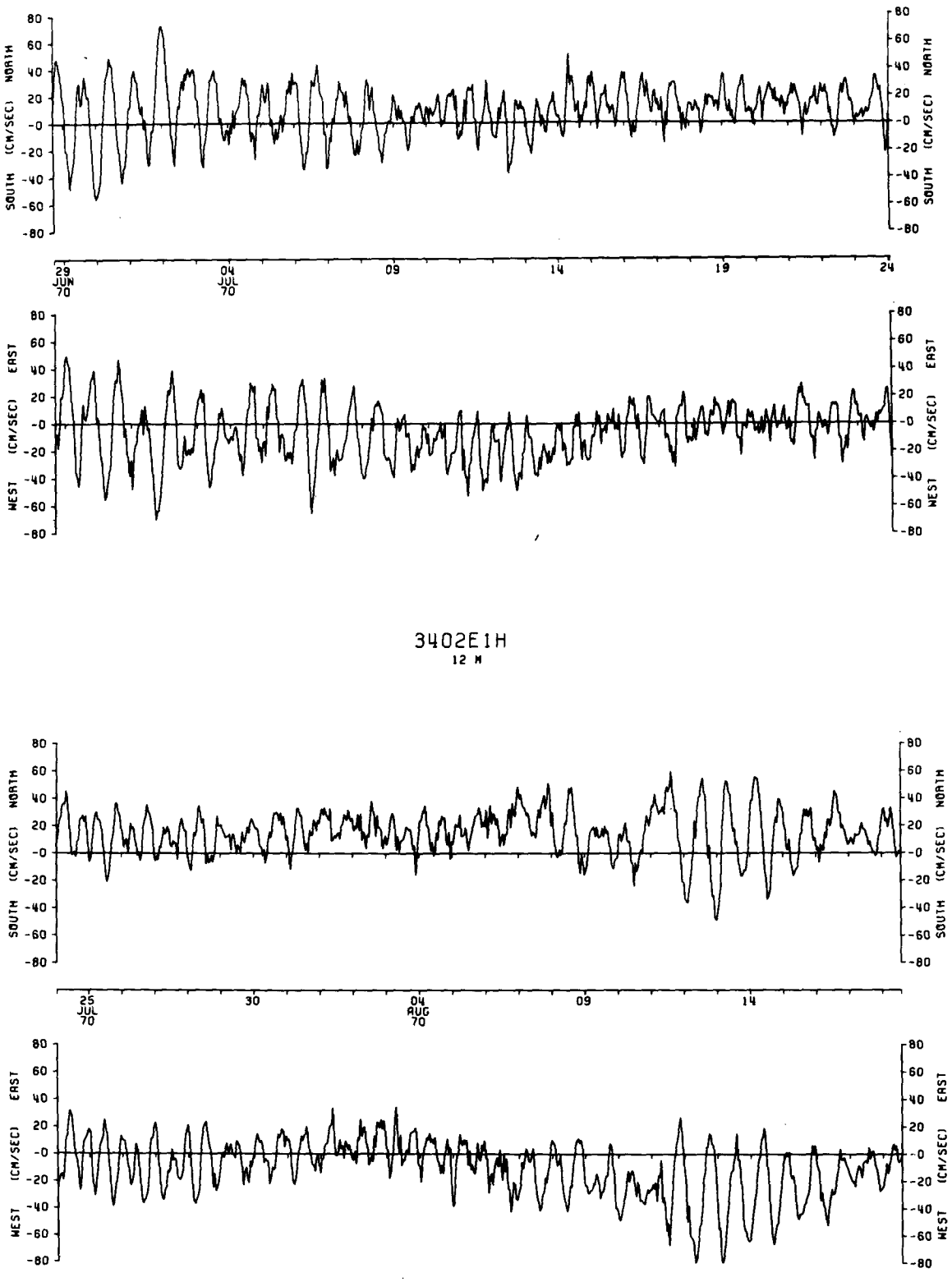

FIG. 3. Cartesian component plots at 12 m depth on mooring 340, using hourly averaged values from record 3402. Both inertial and semidiurnal oscillations can be seen dominating the record at various times.

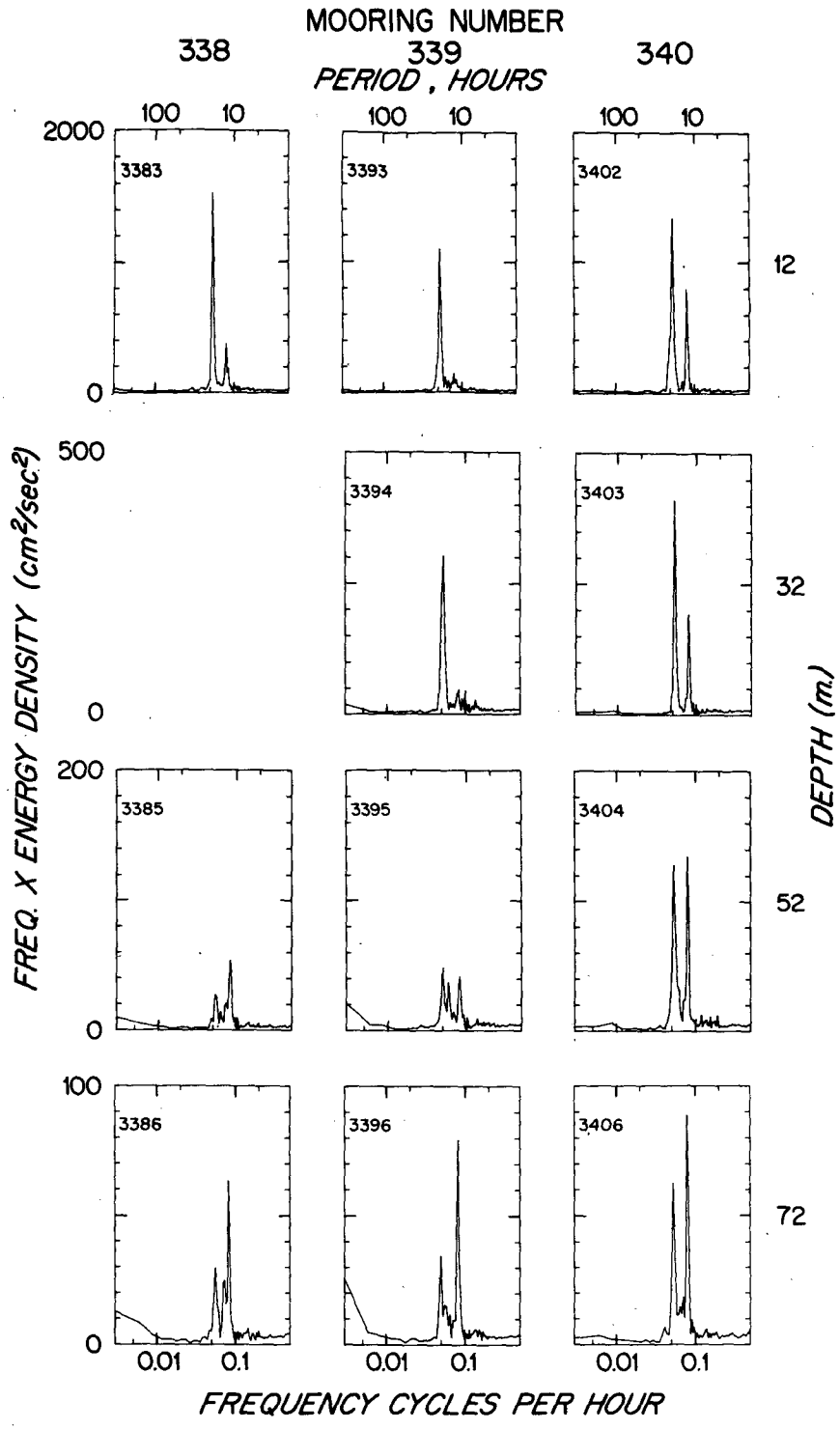

FIG. 4. Spectra of all records in the top 100 m using 1024 h of data between 28 June and 10 August. The abscissa is log-frequency on the lower scale, log-period on the upper scale of each plot. The ordinate is the energy density, scaled by the frequency, plotted linearly. Note that the energy scale is different at different depths, but the same for all records at a fixed depth. The area under this plot in any given frequency band is proportional to the energy in that band. Dominant peaks are inertial (18.78 h) and tidal (12.42 h).

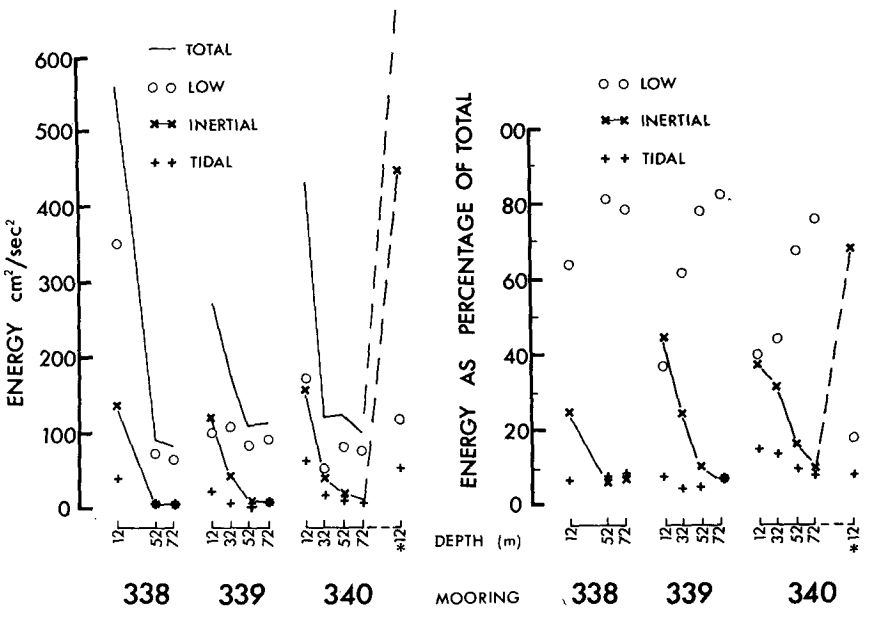

FIG. 5. Partition of energy for the 1024 h period from 1700 GMT 28 June to 0800 GMT 10 August (but the asterisk indicates the 256 h period from 1700 GMT 28 June to 0800 GMT 9 July). The frequency bands are defined by low (mean plus periods from infinity to 25.3 h), inertial (25.3–13.9 h), tidal (13.9–9.9 h) and high (9.9–2.0 h). For clarity, the high-frequency band has not been plotted. It is badly contaminated by aliased surface wave energy but its energy content is still, with one exception, less than that in the tidal band, and it never contributes more than 10% of the total energy.

inertial oscillations dominate, figures are also given for record 3402 for the first 256 h of data. During this period a single burst of storm-generated inertial energy dominated the record. The inertial energy is nearly three times greater than the 1024 h value and constitutes 68%, or two-thirds of the total kinetic energy at the time. During periods of momentum exchange from the atmosphere to the ocean, inertial waves may thus constitute the dominant part of the oceanic response.

To examine the detailed behavior of the amplitude and phase of the inertial oscillations as functions of time, complex demodulation (Perkins, 1970; Pollard and Tarbell, 1975) will be used in later sections. Figs. 8–10 (for all records in moorings 338, 339 and 340, respectively) and Fig. 11 (all 12 m records) have been composited from the complex demodulation plots given in Pollard and Tarbell, but both the phase and amplitude curves have been deleted when the amplitudes are insignificant. This was done subjectively by scanning the east and north component plots (e.g., Fig. 3) and retaining only those portions of the demodulated curves where near-inertial-period oscillations could be discerned by eye on the component plots. The effect of such deletions is to tidy the phase diagrams in particular, since the phase frequently becomes erratic when the amplitudes are insignificant. Since the noise level generally decreases with depth, the low-amplitude cutoff tends to decrease also.

To discuss the dispersion of internal waves a knowledge of the stratification is required. Vertical profiles of Brunt-Väisälä frequency computed from STD surveys on three occasions (Fig. 6) show the effect of summer heating. The stratification increased through July and a mixed layer is well defined only in the August profiles. Significant differences in stratification and mixed-layer depth between the three moorings are apparent, particularly at the end of July.

3. Coherence and dispersion

For the period from 28 June to 10 August, coherence calculations were made for all possible pairs of vertically or horizontally separated instruments (Fig. 7). With 1024 data points at hourly intervals, averaged over 14 adjacent frequency bands about the inertial frequency, there are 28 degrees of freedom, and the 95% confidence level is 0.45. The number of degrees of freedom is suspect because the near-surface records are dominated by the single event during the first week, and the 95% value calculated with the usual assumptions of inde-

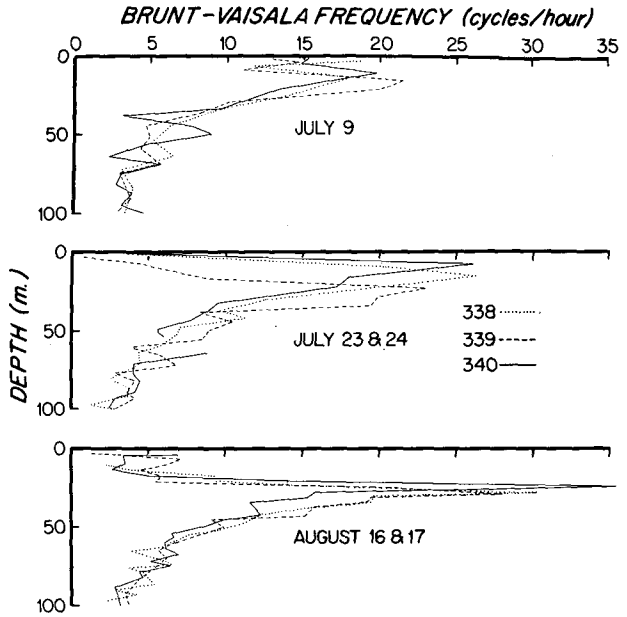

FIG. 6. Brunt-Väisälä frequency at the three moorings on 9 and 23/24 July and 16/17 August as functions of depth in the top 100 m. The profiles were computed using averaged values of density at approximately 5 m intervals, so details of the structure particularly in the top 15 m, have been smoothed.

pendence (which are here violated) is given as a guide only.

Nevertheless, it is clear that, at 50 and 70 km horizontal separation, the records at 12 m are highly coherent (0.8) in the inertial frequency band. In the mixed layer, therefore, the horizontal coherence scale may be significantly larger than the "few tens of kilometers" repeatedly suggested in the literature (Munk and Phillips, 1968; Kundu, 1976; Käse and Olbers, 1979; Webster, 1968; Schott, 1971).

Horizontal coherence falls rapidly with depth. The records at 32 m are still coherent (0.7) but there is no coherence at 52 m (0.2–0.5) or 72 m (0.2–0.4). This implies that input of inertial energy at the surface has the large scales one expects if it is generated by large-scale atmospheric systems. Within a few tens of meters in depth, the oscillations adjust to the smaller oceanic scales of coherence. How is this accomplished?

The answer, we believe, is to be found in the small amplitude of the group velocity, and its sensitivity to variations in N^2 (Fig. 6) and the vertical wavenumber. First, we derive estimates of the group velocity. The dispersion relation for internal inertial waves is

$$(l^2 + m^2)N^2 = n^2(\omega^2 - f^2), \qquad (3.1)$$

where the wavenumber $\kappa = (l,m,n)$, N ($\gg\omega$) is the Brunt-Väisälä frequency and f the inertial frequency. For the group velocity, this yields

$$\mathbf{c}_g = \frac{N^2}{n^2\omega}\left[l, m, \frac{-(l^2 + m^2)}{n}\right]. \qquad (3.2)$$

Note that the vertical component of the group

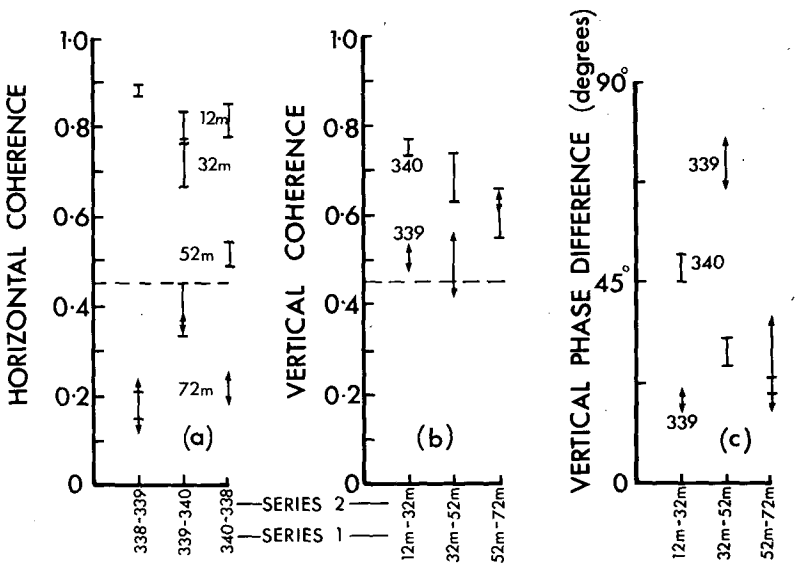

FIG. 7. Coherence and phase of frequencies between $(20.89)^{-1}$ and $(16.25)^{-1}$ cph. For each pair of vector time series, four values of coherence and phase can be calculated (Webster, 1968). Each vertical bar joins the minimum and maximum of the four values. Horizontal coherence values (a) are given for pairs of records at the same depth on different moorings. Vertical coherence (b) and phase (c) are given for pairs of records on the same mooring 20 m apart. Phases are modified by ±90° (cf. Webster, 1968) to give the angle by which the second series leads the first series. The 95% limit for the coherence is 0.45 (but see text).

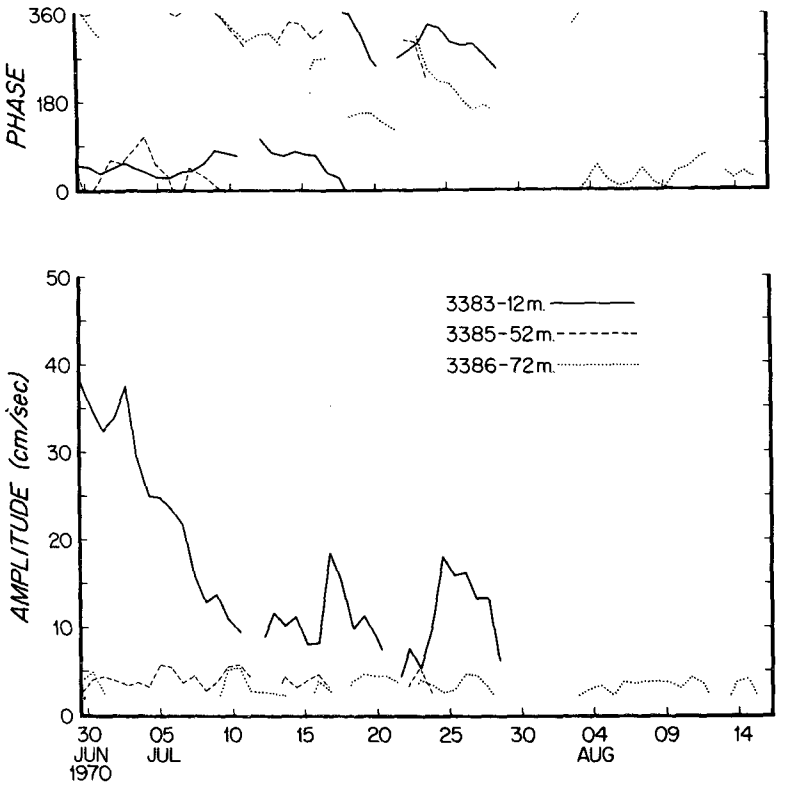

FIG. 8. Amplitude and phase of inertial oscillations as functions of time for the 12, 52 and 72 m records on mooring 338. Values are those found by least-squares fitting a clockwise rotating velocity vector of 18.78 h period to the observed velocity vector using 37.56 h of data. Tidal and low frequencies are removed by the technique. Curves are deleted when the amplitude is insignificant. Phase is defined as the angle by which the rotating vector lags a reference rotating vector of exactly inertial frequency. Thus, if the phase (i.e., lag) decreases as time increases, the observed frequency is greater than inertial.

velocity is proportional to N^2 and n^{-3}, and is directed downward if the vertical phase velocity ωn^{-1} is upward. Using the phase relationships in Figs. 7–11 to estimate wavenumbers and (3.2) to estimate group velocities, the following observations can be made:

1) During the periods of surface generation of inertial oscillations (30 June–6 July, 14–17 August) the phase progression of near-inertial oscillations (Figs. 8–10) is without exception upward, i.e., the phase at each depth is up to a few tens of degrees smaller than that at the next shallower depth. This is confirmed statistically in Fig. 7c in which, for significant values of vertical coherence (Fig. 7b) the phase differences all lie between 20 and 70°. The vertical component of the group velocity is thus directed downward, and the inertial oscillations at 32, 52 and 72 m are wind-forced oscillations dispersing away from the surface. More recent experiments by Kundu (1976), Leaman (1976), Perkins and Van Leer (1977) and Kase and Olbers (1979) have found similar behavior.

2) At 12 m the inertial oscillations at mooring 338 lead those at 339 by 15–35° near the start of the record (Fig. 11). Similarly, 339 leads 340 by 15–40°. Estimating horizontal wavelengths from these figures, one arrives at 700–1700 km, with a direction of propagation to the southwest. Similar scales are suggested by the phase differences associated with the horizontal coherence calculations (not shown in Fig. 7).

3) Phase differences between pairs of records vertically separated by 20 m are typically 30–75° (100–240 m vertical wavelength) during the period of large inertial oscillations at the start of July. At the onset of the oscillations the phase differences may be smaller (10°, 700 m vertical wavelength), consistent with the n^{-3} dependence of the vertical group velocity (3.2).

4) Using the above ranges of values to compute maximum and minimum group velocities, we find that c_{gH}, the horizontal component of $\mathbf{c}_g$, lies between 1 and 20 km day^{-1} (1–20 cm s^{-1}) to the southwest, and the vertical component c_{gv} of $\mathbf{c}_g$ lies between 0.03 and 3 m day^{-1} (3×10^{-5}–3×10^{-3} cm s^{-1}). It is suggested that these small values explain

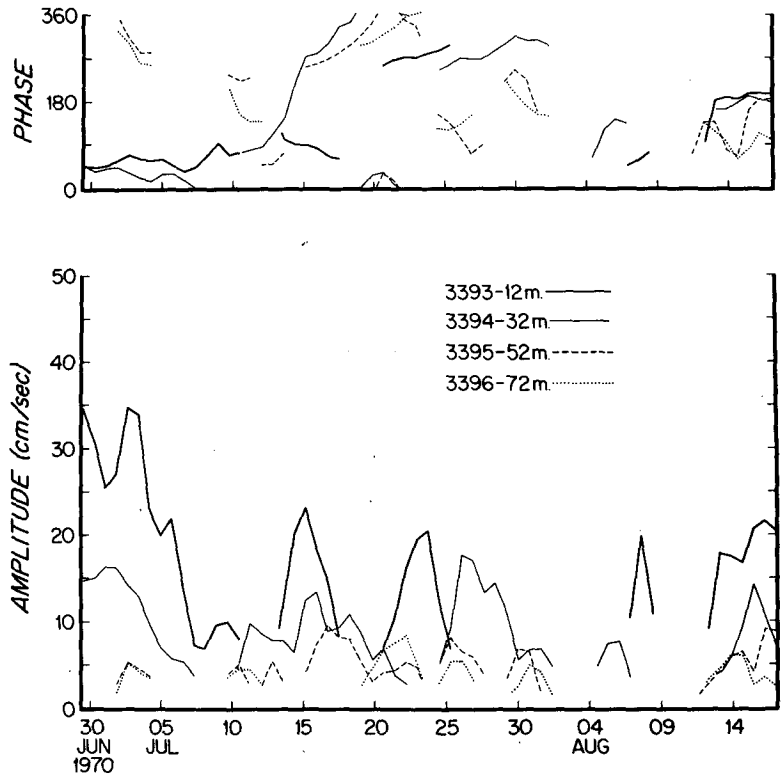

FIG. 9. As in Fig. 8 except for the 12, 32, 52 and 72 m records on mooring 339.

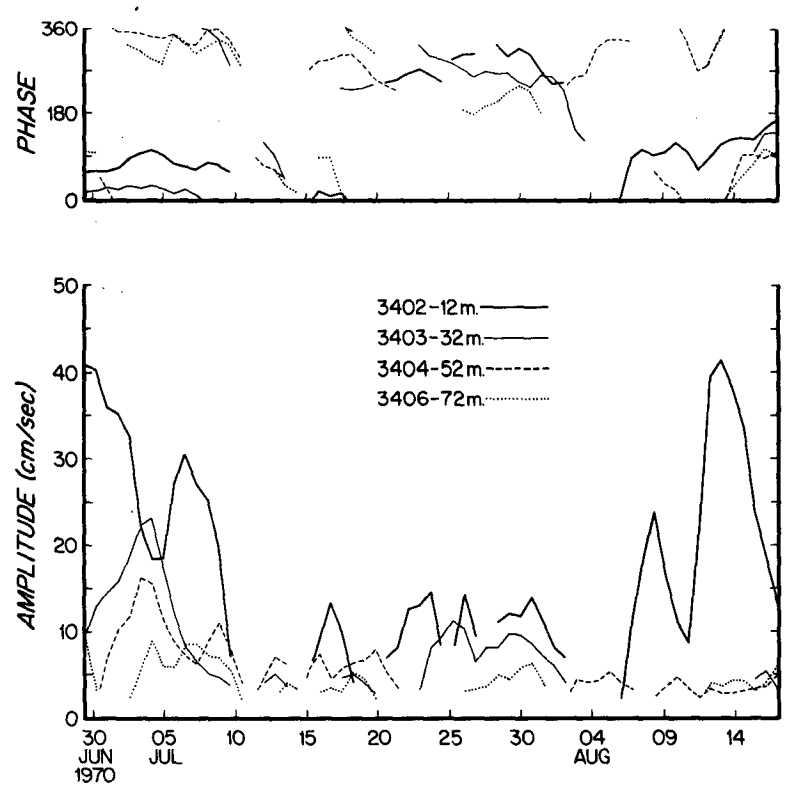

FIG. 10. As in Fig. 8 except for the 12, 32, 52 and 72 m records on mooring 340.

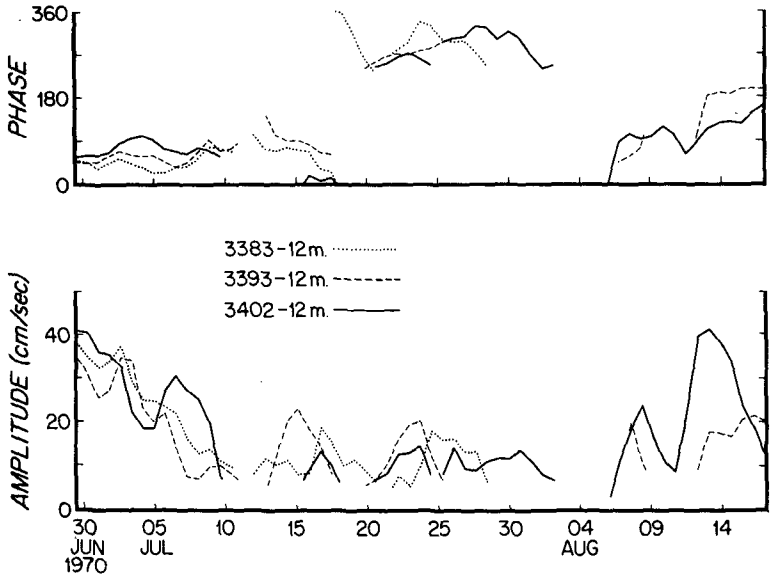

FIG. 11. As in Fig. 8 except for the 12 m records on moorings 338, 339 and 340.

the rapid loss of horizontal coherence with depth. Using the maximum estimates of c_g it takes 6–7 days for near-inertial energy to propagate 20 m vertically, and 3–4 days to travel from one mooring to another. During these several-day periods and over tens of kilometers the variability in the upper ocean reduces the coherence of the inertial motions. The group velocity is sensitive to N^2, which varies by a factor of 2 between moorings (Fig. 6). Kelvin-Helmholtz instability (e.g., Pollard *et al.*, 1973) and turbulence (Bell, 1978) may remove energy from the inertial oscillations. Horizontal advection by depth-varying and horizontally varying mean currents (Pollard and Tarbell, 1975, p. 75) of similar amplitude (10 cm s^{-1}) to the group velocity also contributes to the coherence loss.

5) Can dispersion alone account for the rate of decay of the surface inertial oscillations? The vertical kinetic energy flux due to dispersion is given by $E_d = \frac{1}{2}\rho\sigma^2 c_g v$, where v is a typical inertial period

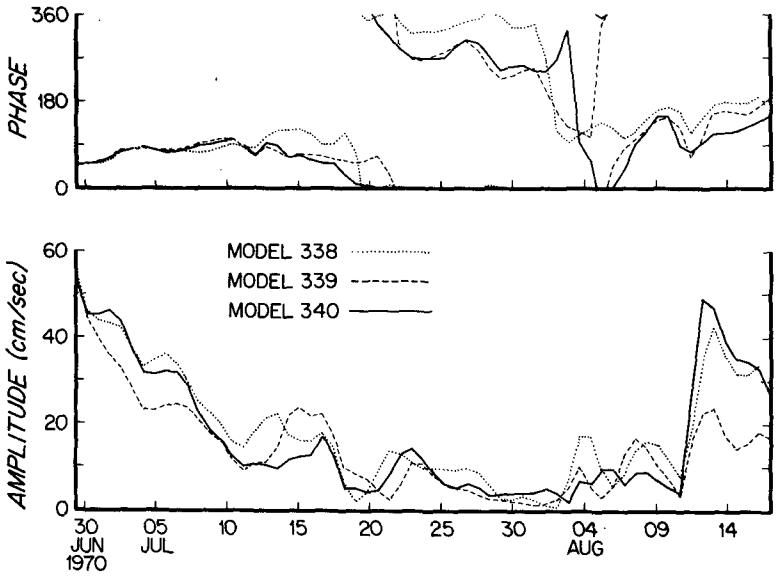

FIG. 12. Amplitude and phase of inertial oscillations as functions of time for the velocity vectors output from the model of Pollard and Millard (1970), using as forcing functions stresses computed from the wind records 3381, 3391 and 3401. Explanation as for Fig. 8 but low amplitudes have not been deleted.

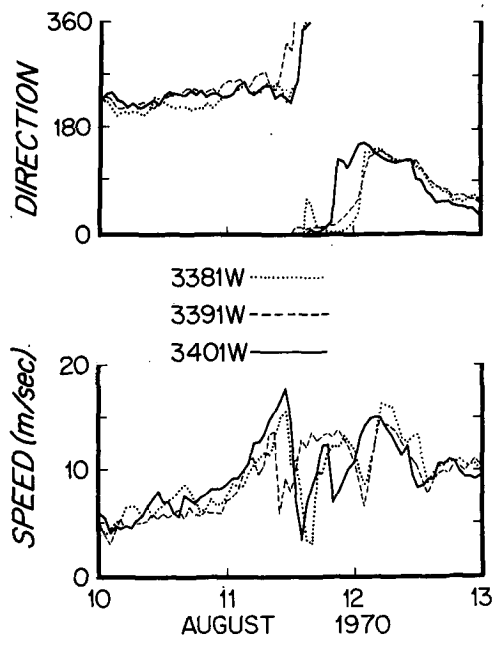

FIG. 13. Wind speed and direction at the three moorings for the period from 10 to 13 August, showing the difference in arrival times of two fronts at the different positions. The 1 h averages used here are barely capable of resolving the passage of the front, but are preferred to 15 min averages which are slightly noise contaminated.

current. Taking mean values appropriate to the period 30 June–5 July (Fig. 11), $v = 30$ cm s^{-1}, $c_{gv} = 1$–3 m day^{-1}, we find $E_d = 0.5$–1.5 erg cm^{-2} s^{-1}, in agreement with previous estimates (Kundu, 1976; Leamann, 1976; Perkins and Van Lear, 1977; Käse and Olbers, 1979).

The actual rate of loss of energy from the mixed layer during the period 30 June–5 July (Fig. 11) can be estimated by $E = \frac{1}{2}\rho(v^2_{\text{initial}} - v^2_{\text{final}})DT^{-1}$, where D is the mixed-layer depth, T the period over which the loss occurs. Taking velocities of 40 cm s^{-1} reducing to 20 cm s^{-1}, $D = 25$ m, $T = 5$ days, we estimate $E = 4$ ergs cm^{-2} s^{-1}, several times larger than E_d. It appears unlikely that dispersion alone can account for the energy loss. Another mechanism, such as that proposed by Bell (1978), must be involved.

4. Surface forcing

We now pass from the dispersive properties of inertial oscillations to consideration of their generation and of the spatial variations of the forced oscillations in the surface layer.

Wind records taken at each of the three moorings (Pollard and Tarbell, 1975) are similar in all their main features, with high coherence at frequencies ≤ 0.08 cph (Gonella, 1972). It is of interest to apply each wind record to the model used by Pollard and Millard (1970), to test 1) the sensitivity of that model to minor wind differences, and 2) whether the model can simulate differences in the inertial oscillations similar to those that were observed between the three mooring positions. This was done using the same initial condition in each case, a 4-day e-folding time for the damping term, a drag coefficient of 0.001 and a mixed-layer depth of 12 m. Complex demodulation centered on the inertial period was applied to the modeled current records (Fig. 12) as well as to the observed currents at 12 m depth (Fig. 11).

It should be stressed that the primary aim of the model is to predict the inertial component of the rapid response (<1 day) of the oceanic surface layer to rather sudden variations in wind stress. On this time scale the damping term is of no consequence. On a longer time scale its only function is to remove energy, however unrealistically, so that only suitably reduced-amplitude oscillations remain as initial conditions for later inertial-generating wind events.

Although the gross features of the three modeled currents (Fig. 12) are similar, they differ at times by 60° or more in phase and a factor of 2 in amplitude. Thus the model is sensitive to small differences in the forcing function.

The modeled inertial oscillations (Fig. 12) are encouragingly similar to those observed (Fig. 11). Unfortunately, the front which generated the large oscillations at the start of the records passed before the moorings were set, so cannot be modeled. Synoptic charts show that an east–west orientated warm front remained in the vicinity of 40°N for some time before the associated cold front passed site D on 27 June. The structure was sufficiently complex that one cannot verify the inertial current amplitude or phase differences found between the three mooring positions in the absence of detailed wind records. The amplitude and phase of the model are initially set to force a good comparison with the observed currents, but the damping term reduces the influence of the initial conditions within a few days. However, the phases of the models continue to follow the observed phase, remaining between 0 and 90° until 19th July, shifting to between 270 and 360° until the end of July, and trending upward from 0 to 180° between 6 August and the end of the record on 17 August.

A number of amplitude maxima, such as that on 339 around 15 July, appear to be reflected in the model, though the comparison is not as striking as for the phases. This is not surprising, because the greatest uncertainty in the model lies in the amplitude factors. The drag coefficient may be wrong. The amplitude decay factor is crude. The mixed-layer depth, kept constant in the model, is definitely a function of time (Fig. 6). The current meter at 12 m was not even in the mixed layer for parts of the

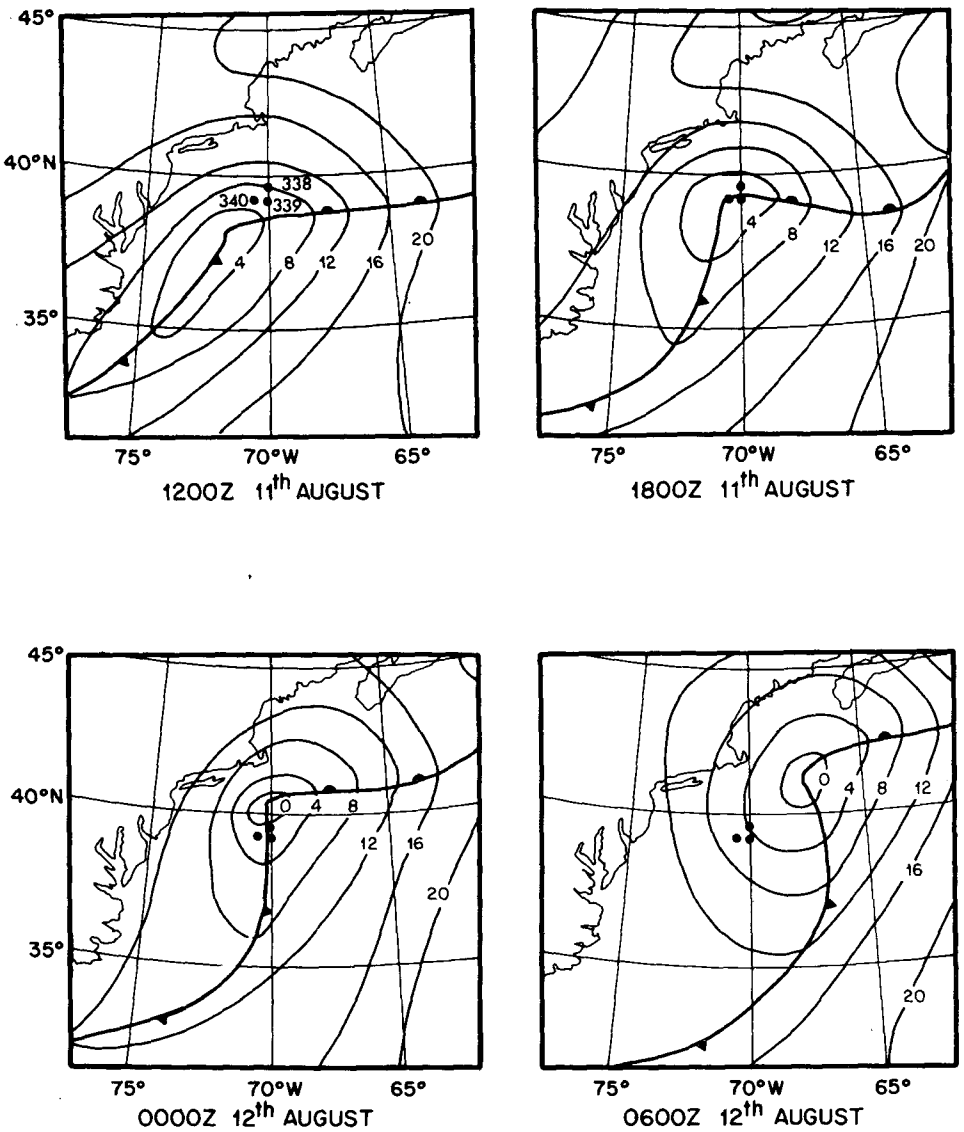

FIG. 14. Synoptic charts centered on site D, taken from the 6 h Northern Hemisphere surface weather charts compiled by the National Weather Service. The moorings are marked by the three dots in the vicinity of 39°N, 70°W. While these charts give a good qualitative picture of the depression with which the fronts of Fig. 13 are associated, they are imprecise as to the exact timing and position of the storm track.

record (Millard, private communication). Nevertheless, there is a marked similarity between observed and computed oscillations from 11 to 17 August which we shall discuss in detail.

Record 3383, which was of poor quality at all times, stops early in August, but the remaining records compare well with the modeled output, both in amplitude ratio and in phase difference. The wind records (Fig. 13) show the passage of two fronts on 11 August, which are shown by synoptic charts (Fig. 14) to be associated with a well-developed northeastward-traveling depression. Since these fronts pass the moorings in the order 340, 339 then 338, the oscillations at 340 lead those at 339 and 338, and therefore have a lower phase (as defined in Fig. 8), both in the modeled and observed records. The amplitudes of the resultant oscillations depend primarily on the duration of the forcing event or the time difference between the arrival of the two fronts at a given mooring. The wind shift in the first front is clockwise from 250° to 0°, in the second from 0° to 135°, which is ideal for inertial wave generation if the time between the fronts is about a third of an inertial period, or 6 h. Since the time differences between the arrivals of the fronts at 340, 338 and 339 were 7, 12 and 16 h, respectively, one expects

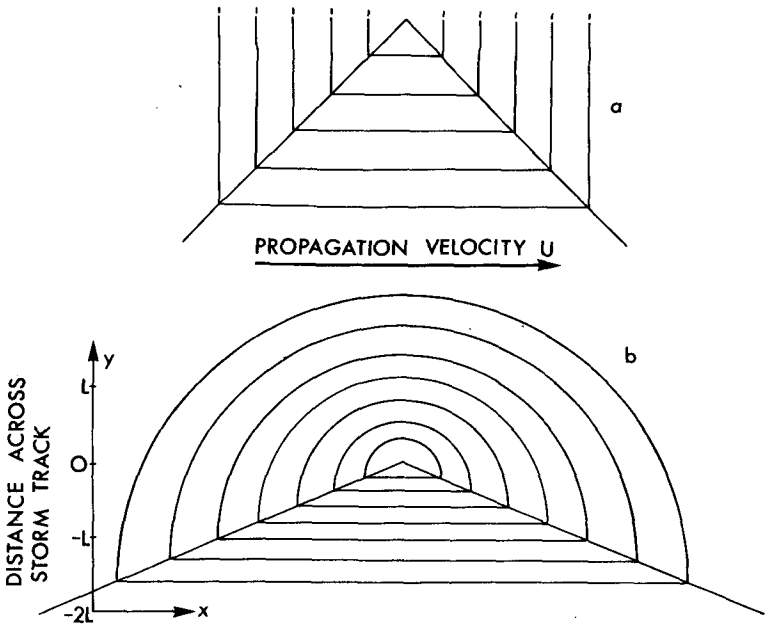

FIG. 15. Isobars corresponding to geostrophic wind fields used to model analytically (a) and numerically (b) the spatial variations in the forced inertial wave field. The depressions are propagating in the x direction with speed U. The isobar separation in Fig. 15b gives a Gaussian y-dependence $\exp[-(y/1.5L)^2]$ to the wind stress, where $L = UP$ and P is the inertial period.

considerably larger amplitudes at 340 than at 339, as is the case in both modelled and observed currents. Thus the ocean is sensitive to small differences in the wind stress.

Since we find the model capable of representing spatial differences, we conclude that only the local wind as a function of time is needed to forecast the initial response of the mixed layer. Accordingly, we can learn something about the spatial behavior of inertial oscillations in the mixed layer using simple approximations to the frontal system in Fig. 14.

Consider the propagating depression modeled by Fig. 15a, whose essential features are the two fronts whose positions at time t are defined by $x - Ut = \pm y$, $y \leq 0$. Consider only $y < 0$. We ignore the component of the wind due to the propagation velocity U, so the stress can be written

$$\tau \equiv (\tau_x,\tau_y) = \begin{cases} \tau_0(0,1), & Ut - x < y \\ \tau_0(1,0), & y < Ut - x < -y \\ \tau_0(0,-1), & -y < Ut - x. \end{cases} \quad (4.1)$$

The equations

$$\frac{\partial u}{\partial t} - fv = \tau_x, \quad \frac{\partial v}{\partial t} + fu = \tau_y \quad (4.2)$$

can be solved at any fixed point (x,y), with the given time dependence of the wind stress. If we take $(u,v) = (\tau_0/f,0)$ at $x = \infty$, the solution becomes

$$(u,v) = (-\tau_0/f, 0) + 2\sqrt{2}\cos\left(\frac{fy}{u} + \frac{\pi}{4}\right) \times \left[\cos f\left(t - \frac{x}{u}\right), -\sin f\left(t - \frac{x}{u}\right)\right], \quad (4.3)$$

when $Ut - x > -y$, i.e., after the fronts have passed.

To supplement the simple analytical expression (4.3), solutions have been obtained numerically (Fig. 16) for the bounded depression of Fig. 15b chosen to model as closely as possible the observed depression described in Figs. 13 and 14.

Eq. (4.3) and Fig. 16 reveal a good deal about the spatial structure of storm-generated inertial waves. In the direction of propagation of the storm system, the wavelength is simply $L \equiv UP$, where P is the inertial period. For the storm of Fig. 14, U is ~500 km day^{-1}, yielding a wavelength $L = 400$ km in the southwest to northeast direction. Changes in amplitude along the storm track depend on the development of the depression with time.

Perpendicular to the storm track the picture is very different. There is no phase change with y [except for 180° phase shifts (Fig. 16b)] and, consequently, no propagation. The oscillations constitute a standing wave whose amplitude variation again has scale L [Eq. (4.3)], or more generally $L/\tan\theta$, where θ is the half-angle between the two

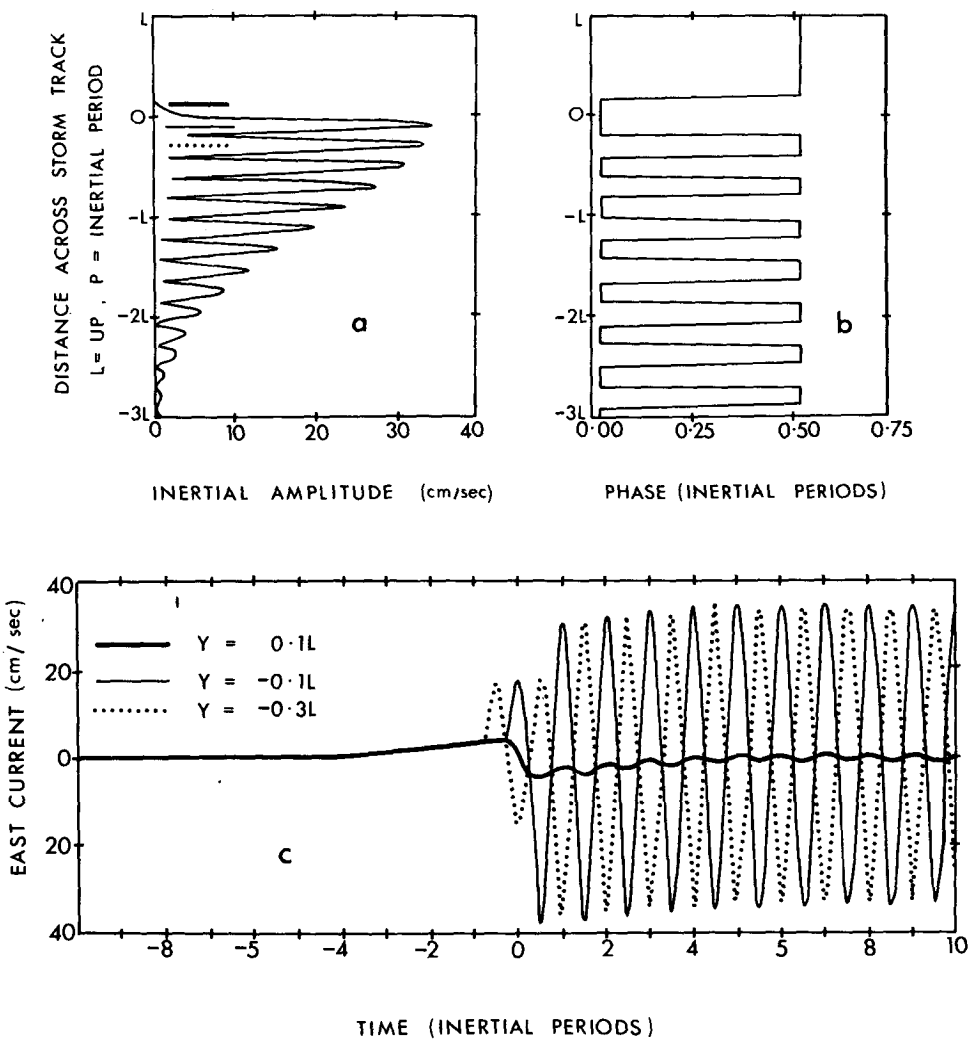

FIG. 16. Currents generated by the depression of Fig. 15b. The amplitude (a) and phase (b) of the inertial oscillations after the depression has passed are shown as functions of distance across the storm track. The east component of the current as a function of time (c) is shown for the three positions marked on (a). The amplitudes are given in cm s^{-1}, but should be thought of as arbitrary units depending on the wind stress, mixed-layer depth and drag coefficient.

fronts. The scale L_y on which the amplitude changes from a maximum value to zero across the storm track can therefore be quite small. For the model of Fig. 15, for example, with $\theta = 67.5°$, $L_y = L/4 \times \tan\theta = 0.1L$ (Fig. 16a) so L_y is only 40 km for $L = 400$ km. For the observed depression (Fig. 14) propagating to the northeast, moorings 339 and 340 are ~35 km apart, measured perpendicular to the storm track, and the inertial current at mooring 340 after the depression has passed (Fig. 11, 12 August) is accordingly more than twice that at mooring 339.

In the absence of fronts, generation of inertial oscillations is much diminished and the amplitude can fall to negligible values within a few tens of kilometers of the center of a depression (Fig. 16a and 16c, $Y > 0$).

We conclude that the generation of inertial oscillations is so sensitive to variations in the wind that they cannot be predicted accurately in the absence of local wind records.

Finally, note that in considering local oscillations generated by the local wind, we have ignored the effect of horizontal divergences within the mixed layer. Across the storm track, for example, a change in the inertial amplitude from 40 to 0 cm s^{-1} in 40 km must cause, for a 40 m mixed layer, vertical excursions of the bottom of the mixed layer of up to ~4 m amplitude, with a horizontal wavelength ($L/\sin\theta$) of 160 km. The forced oscillations are therefore coupled to the thermocline, the frequency must be slightly greater than inertial and dispersion will occur.

5. Summary

Inertial waves are generated intermittently in both space and time by wind stress on the ocean surface. Forcing is most efficient in depressions, particularly along fronts. The response at inertial frequencies is sensitive to variations in the local wind from place to place, but the spatial variations in the response can be modeled using the equations developed by Pollard and Millard (1970) with forcing by the local wind. Once generated, these packages of energy decay by slow downward dispersion, spreading horizontally at the same time. Dispersion alone does not appear to be large enough to account for the decay rate of the near surface oscillations, and is probably supplemented by destruction by changes in the local wind (e.g., Pollard and Millard, 1970) and by conversion to higher frequency oscillations (Bell, 1978).

Inertial motions adjust from the large horizontal scales appropriate to meteorological forcing to much smaller oceanic scales within a few tens of meters of the surface. Small vertical group velocities (of order 1 m day^{-1}) give time for the natural variability in the upper ocean (turbulence, advection, Kelvin-Helmholtz instability) to reduce the horizontal coherence during the few days it takes for energy at near-inertial frequencies to penetrate a few tens of meters. The group velocities are themselves sensitive to the local stratification (N^2) and the vertical wavenumber.

Acknowledgments. The data analyzed in this paper were collected by the Buoy Group of the Woods Hole Oceanographic Institution, supported by the Office of Naval Research under Contract N00014-66-C0241. The author is most appreciative of the considerable amount of help and cooperation which many individual members of this group have given him, in particular Mr. R. C. Millard, who undertook the major task of collecting and reducing the stratification data. Some of the data analysis was done with the help of Mr. G. Alexander at Southampton University, where the author was supported by the Natural Environment Research Council under Contract F/60/6/3. The author was supported by the Office of Naval Research under Contract N00014-66-C0241 and the National Science Foundation under Contract NSF 10208 while preparing the first draft of this paper.

REFERENCES

Bell, T. H., 1978: Radiation damping of inertial oscillations in the upper ocean. *J. Fluid Mech.*, **88,** 289–308.

Gonella, J., 1971: A local study of inertial oscillations in the upper layers of the oceans. *Deep-Sea Res.*, **18,** 775–788.

——, 1972: A rotary-component method for analysing meteorological and oceanographic vector time series. *Deep-Sea Res.*, **19,** 833–846.

Halpern, D., 1974: Observations of the deepening of the wind-mixed layer in the north east Pacific Ocean. *J. Phys. Oceanogr.*, **4,** 454–466.

Käse, R. H., 1979: Calculations of the energy transfer by the wind to near-inertial internal waves. *Deep-Sea Res.*, **26,** 227–232.

——, and D. J. Olbers, 1979: Windstress-forced inertial waves during GATE. *Deep-Sea Res.*, GATE volume (in press).

Kroll, J., 1975: The propagation of wind-generated inertial oscillations from the surface into the deep ocean. *J. Mar. Res.*, **33,** 15–51.

Kundu, P. K., 1976: An analysis of inertial oscillations observed near Oregon coast. *J. Phys. Oceanogr.*, **6,** 879–893.

Leaman, K. D., 1976: Observations on the vertical polarization and energy flux of near-inertial waves. *J. Phys. Oceanogr.*, **6,** 894–908.

Munk, W., and N. Phillips, 1968: Coherence and band structure of inertial motion in the sea. *Rev. Geophys.*, **6,** 447–471.

Perkins, H. T., 1970: Inertial oscillations in the Mediterranean. Ph.D. thesis, MIT-WHOI Joint Program.

——, and J. Van Leer, 1977: Simultaneous current-temperature profiles in the equatorial counter current. *J. Phys. Oceanogr.*, **7,** 264–271.

Pollard, R. T., 1970: On the generation by winds of inertial waves in the ocean. *Deep-Sea Res.*, **17,** 795–812.

——, and R. C. Millard, 1970: Comparison between observed and simulated wind-generated inertial oscillations. *Deep-Sea Res.*, **17,** 813–821.

——, and S. Tarbell, 1975: A compilation of moored current meter and wind observations, Vol. VIII (1970 array experiment). WHOI Ref. 75-7 (unpublished manuscript).

——, P. B. Rhines and R. O. R. Y. Thompson, 1973: The deepening of the wind-mixed layer. *Geophys. Fluid Dyn.*, **3,** 381–404.

Schott, F., 1971: Spatial structure of inertial-period motions in a two-layered sea, based on observations. *J. Mar. Res.*, **29,** 85–102.

Webster, F., 1968: Observations of inertial-period motions in the deep sea. *Rev. Geophys.*, **6,** 473–490.